Supporting Information

Synthesis of Dendritic Pt-Ni-P Alloy Nanoparticles with Enhanced Electrocatalytic Properties

Jingfang Zhang, Kaidan Li, Bin Zhang[*]

Department of Chemistry, School of Science, Tianjin University, and Collaborative Innovation Center of Chemical Science and Engineering (Tianjin), Tianjin 300072, China.

Corresponding Author * E-mail: bzhang@tju.edu.cn

EXPERIMENTAL SECTION

1. Catalyst Preparation. Dendritic Pt-Ni-P alloy nanoparticles (NPs) were prepared by a wet-chemical route. In a typical synthesis, 0.05 g F68 ($(C_3H_6O \cdot C_2H_4O)_x$) was dissolved in 10 mL of water. After being thoroughly dissolved, 4 mL 10 mM K_2PtCl_4 solution was added. Then 4 mL 0.05 M aqueous ascorbic acid (AA) solution was quickly added. The mixture solution was further stirred for 4 hours at room temperature. Next, appropriate amounts of $NiCl_2$ and NaH_2PO_2 solutions were added in turn into the above solution under stirring (The relative molar quantities of $NiCl_2$ and NaH_2PO_2 were adjusted in this study, yielding six distinct samples, which are summarized in Table S1.) before adding a freshly prepared aqueous $NaBH_4$ solution (2 mL, 0.2 M). The results solution was kept at room temperature for 10 min. The products were collected by centrifugation at 12000 rpm for 5 min, and washed several times with 0.5 M H_2SO_4 solution, water, and ethanol, then dried at 40 °C in a vacuum oven for 12 h.

Table S1. Reactant Ratios for the Synthesis of Various Samples

Sample No.	Relative reactant molar quantities			Named as
	K_2PtCl_4	$NiCl_2$	NaH_2PO_2	
1	8.0	1	18.8	PtNiP (our sample)
2	16.0	1	37.6	Sample 2
3	5.3	1	12.5	Sample 3
4	8.0	1	9.4	Sample 4
5	8.0	1	28.2	Sample 5
6	8.0	1	—	PtNi

2. Electrochemical Measurements. Electrochemical measurements were carried out in a typical three-electrode cell consisting of a working electrode, a Pt wire counter electrode, and a saturated calomel reference electrode (SCE) performed using an electrochemical workstation (CHI 660D, CH Instruments, Austin, TX). A glassy carbon electrode (diameter d = 3 mm, Tianjin Incole Union Technology Co .,Ltd) was used as the working electrode. The electrode was firstly polished with Al_2O_3 powders with size down to 0.05 μm. Prior to the deposition of catalysts, the electrode was thoroughly rinsed with Ultrapure Millipore water and ethanol three times to remove contaminants, respectively. All potentials, if not specified, were recorded according to reversible hydrogen electrode (RHE) in this work. For Pt-Ni-P and Pt-Ni catalysts working electrode, 1 mg of various composition ratios of Pt-Ni-P and Pt-Ni catalysts were dispersed in 2 mL of a mixture solvent (the volume ratio of H_2O: isopropanol: 5% Nafion is 4 : 1 : 0.025), and the mixture was sonicated for 40 min to get a homogeneous ink. For commercial Pt/C (20 wt%, Johnson Matthey) working

electrodes, 5 mg Pt/C catalysts (containing 1 mg Pt) was used with other conditions remaining unchanged. Then 4 μL of the ink was dropped onto the working electrode and dried in flowing argon for all catalysts.

Specifically, cyclic voltammetrys (CVs) were performed in 0.5 M N_2-purged H_2SO_4 solution at a scan rate of 50 mV s^{-1}. The electrochemically active surface areas (ECSAs) of the catalysts can be calculated from the electric charges of H_{upd} adsorption with an assumption of 210 μC cm^{-2} for the adsorption of a monolayer of hydrogen.

For methanol oxidation and formic acid oxidation, CVs were recorded in 0.5 M H_2SO_4 + 0.5 M CH_3OH and 0.5 M H_2SO_4 + 0.5 M HCOOH, respectively, at a scan rate of 50 mV s^{-1}.

Chronoamperometry was carried out in 0.5 M H_2SO_4 + 0.5 M CH_3OH at a potential of 0.79 V (vs. RHE) for methanol oxidation, and in 0.5 M H_2SO_4 + 0.5 M HCOOH at 0.89 V (vs. RHE) for formic acid oxidation.

For CO stripping, high-purity CO was bubbled into 0.5 M H_2SO_4 for 30 min while holding the electrode potential at 0.24 V (vs. RHE). Dissolved CO was then purged out of the electrolyte by bubbling N_2 for 30 min. Two consecutive CVs were recorded for the catalysts between -0.01 and 1.24 V (vs. RHE) at a scan rate of 50 mV s^{-1}.

3. Characterization. The scanning electron microscopy (SEM) images were taken with a Hitachi S-4800 scanning electron microscope. Transmission electron microscopy (TEM), high-resolution transmission electron microscopy (HRTEM) images were obtained with FEI Tecnai G2 F20 system equipped with GIF 863 Tridiem (Gatan), and energy-dispersive X-ray spectroscopic (EDX) elemental distribution images were determined by JEM 2100F transmission electron microscope. Specimens for TEM and HRTEM measurements were prepared via dropcasting a droplet of ethanol suspension onto a copper grid, coated with a thin layer of amorphous carbon film, and allowed to dry in air. The X-ray diffraction (XRD) patterns of the products were recorded with Bruker D8 Focus Diffraction System using a Cu Kα source (λ = 0.154178 nm) at a scan rate of 2 degree (2θ) /min. X-ray photoelectron spectrum (XPS) analysis was performed on a PHI 5000 Versaprobe

system using monochromatic Al Kα radiation. All binding energies were referenced to the C 1s peak at 284.8 eV. ICP-MS (Agilent 7700x, USA) was used to determine the compositions of the products.
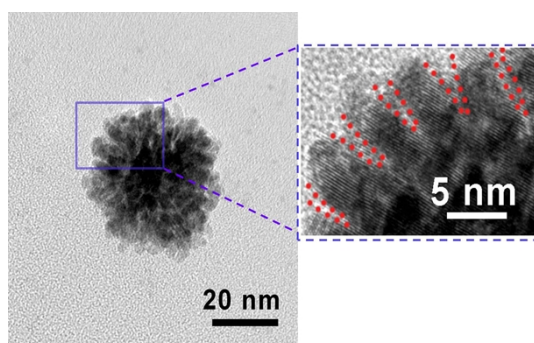

Fig. S1 TEM images of dendritic Pt-Ni-P NPs (left) and enlarged image of the square area (right).

From the enlarged TEM image, we can see the nanosphere consists of a number of interconnected branches instead of nanoparticles. To make a clearer observation, we use red dash lines for outlining the voids between branches.
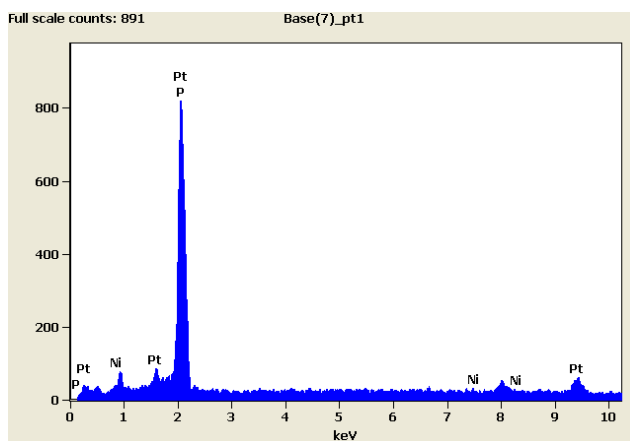

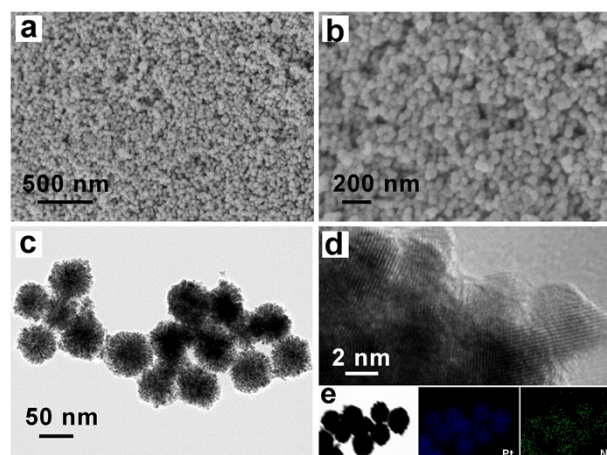**Figure S2.** EDX spectrum of the dendritic Pt-Ni-P NPs.

Figure S3. (a-d) Representative low (a) and high (b) magnification SEM, TEM (c), HRTEM (d) images of the dendritic Pt-Ni NPs. (e) The corresponding TEM image and elemental mapping images showing the distribution of Pt (blue) and Ni (green).

Figure S3a-b show the representative SEM images of dendritic Pt-Ni NPs. Most of the typical products had a roughly spherical shape with high yield. From TEM images (Figure S3c), the products are dendritic NPs with multiple arms. The average diameter is 58 nm, which is larger than that of dendritic Pt-Ni-P NPs. We can conclude that the incorporation of P can decrease the size of NPs. Figure S3d shows the HRTEM image of dendritic Pt-Ni NPs. The different lattice orientations confirm the polycrystalline character of the dendritic nanostructures. The EDX elemental mapping images (Figure S3e) indicate that Pt and Ni are distributed uniformly throughout the entire dendritic NPs.
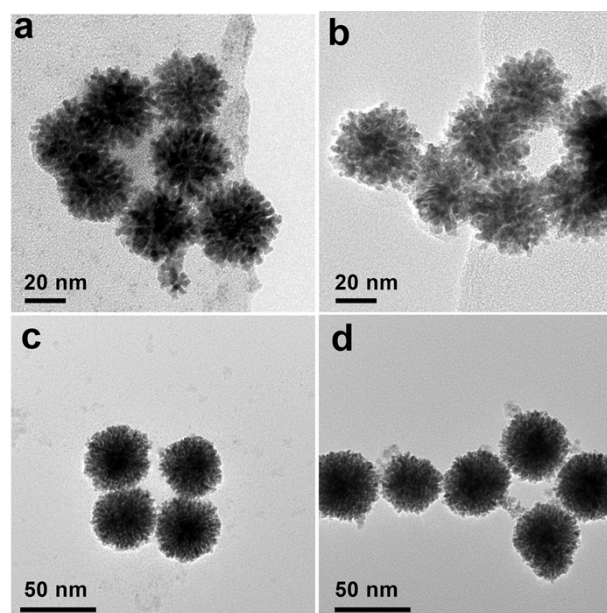

Figure S4. TEM images of the samples collected during the synthesis of dendritic Pt-Ni-P NPs. (a) TEM image of dendritic Pt NPs before adding $NiCl_2$ and NaH_2PO_2. The synthesis was run for 1min (b), 5min (c) and 10 min (d) after $NaBH_4$ is added to the reaction system at t = 4 h.

Dendritic Pt NPs are firstly obtained in a simple reaction system at t = 4 h (Figure S4a). The images indicate that the branched NPs have an average size of 34 nm. The average size of the nanostructures increased to 38 nm at the first minute and to 41 nm at five minutes (Figure S4b,c). Beyond five minutes, no further change in the size or the morphology of the nanostructures was observed (Figure S4d).
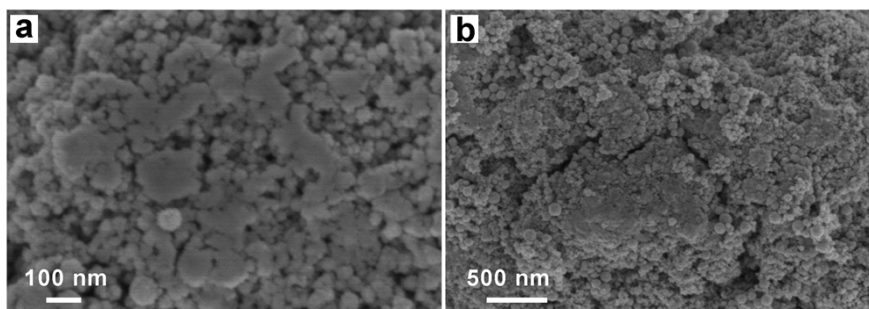

Fig. S5 (a, b) Representative SEM images of the products collected from the reaction with the similar condition used in the synthesis of dendritic Pt NPs but in the absence of F68.

The images show that the obtained product is irregularly shaped bulk rather than mono-dispersed nanospheres. Hence, it was proved that F68 plays a critical role in directing the formation of dendritic nanostructures.
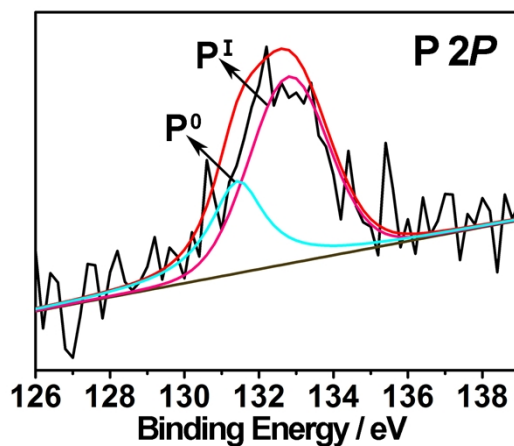

Figure S6. XPS spectrum of the P 2p region for dendritic Pt-Ni-P NPs.

In the P 2p spectrum of dendritic Pt-Ni-P NPs, the peaks at 131.4 and 132.8 eV are assigned to elemental state P^0 and oxidized phosphorus, respectively. The positive shift about 1.0 eV compared with pure P^0 (130.4 eV) in the lower binding energy of P 2p indicated the change of atomic and electronic structure due to the formation of Pt-Ni-P alloy.

Table S2. Specific peak positions collected from the XRD data

materials	Plane(111)	Plane(200)	Plane(220)	Plane(311)	Plane(222)
Pure Pt	39.763	46.243	67.454	81.286	85.712
PtNi	39.916	46.327	67.857	81.499	86.301
PtNiP	39.814	46.324	67.737	81.319	85.903

Table S3. The corresponding chemical compositions results based on EDX spectra

Materials	Pt: Ni: P (atomic ratio)
Sample 2	82.20%: 2.38%: 15.42%
Sample 3	73.56%: 10.42%: 16.02%
Sample 4	80.65%: 6.61%: 12.74%
Sample 5	63.45%: 5.29%: 31.25%

By adjusting the molar quantities of $NiCl_2$ and NaH_2PO_2 involved in the system (Table S1), dendritic Pt-Ni-P alloy samples with different compositions were prepared. Among them, sample 2 and 3 were used to control the amount of Ni, and sample 4 and 5 were used to control the amount of P. The corresponding chemical compositions results based on EDX spectra are listed in Table S3.

Table S4. Integrated charges and ECSAs for PtNiP, PtNi and Pt/C collected from CV curves for H_{upd} (Q_H), CO stripping (Q_{CO}), and the ratio between measured charges

Materials	Q_H [μC]	$ECSA_H$ [cm^2]	Q_{CO} [μC]	$ECSA_{CO}$ [cm^2]	$Q_{CO}/2Q_H$
PtNiP	157	0.75	324	0.77	1.03
PtNi	123	0.59	251	0.60	1.02
Pt/C	168	0.80	333	0.79	0.99

For each PtNiP and PtNi samples, the ratio ($Q_{CO}/2Q_H$) between the charges for CO stripping and H_{upd} is close to 1:1, similar to Pt/C. The difference between ECSAs obtained from CO stripping and H_{upd} is not obvious mainly because there is no formation of Pt-skin type of surface over PtNi and PtNiP samples. Considering that the $ECSA_{CO}/ECSA_H$ ratio (1:1) and the popularity of H_{upd} method, the specific current density was normalized to the $ECSA_H$ measured by the H_{upd} adsorption method. The

ECSAs were calculated as 55.95 $m^2\ g_{Pt}^{-1}$ for dendritic Pt-Ni-P alloy NPs, 32.56 $m^2\ g_{Pt}^{-1}$ for dendritic Pt-Ni alloy NPs, and 61.69 $m^2\ g_{Pt}^{-1}$ for commercial Pt/C.
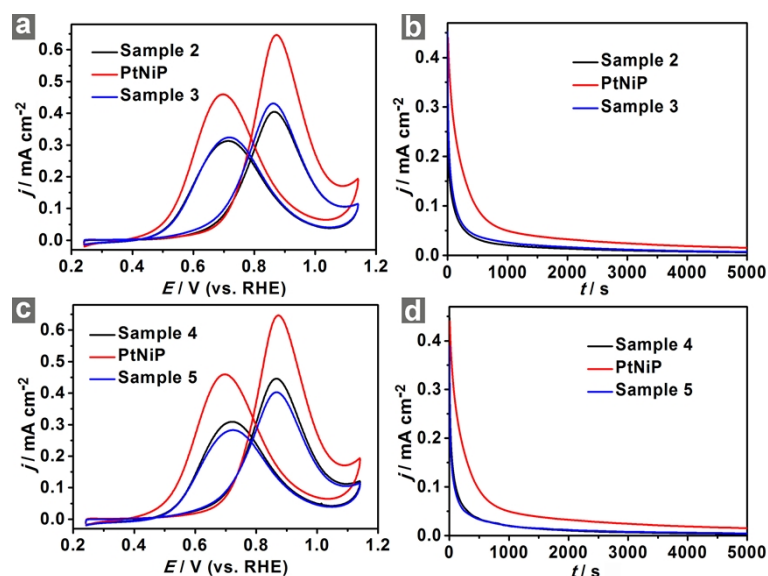

Figure S7. (a, b) Specific activities (a) and chronoamperometry curves (b) of as-prepared dendritic Pt-Ni-P alloy NPs, sample 2, and sample 3 recorded in 0.5 M H_2SO_4 + 0.5 M CH_3OH solution at a scan rate of 50 mV s^{-1}. (c, d) Specific activities (c) and chronoamperometry curves (d) of as-prepared dendritic Pt-Ni-P alloy NPs, sample 4, and sample 5 recorded in 0.5 M H_2SO_4 + 0.5 M CH_3OH solution at 0.79 V.

Figure S7a and S7c show the specific activities normalized to ECSAs in 0.5 M H_2SO_4 + 0.5 M CH_3OH solution at 50 mV s^{-1}. It can be seen that the dendritic Pt-Ni-P alloy NPs (our sample) exhibits higher activity than other composition samples. In addition, as indicated by chronoamperometry curves at 0.79 V (Figure S7b and S7d), the dendritic Pt-Ni-P alloy NPs demonstrated a higher specific current densities and a slower current decay than that of other composition samples, showing better stability in MOR.
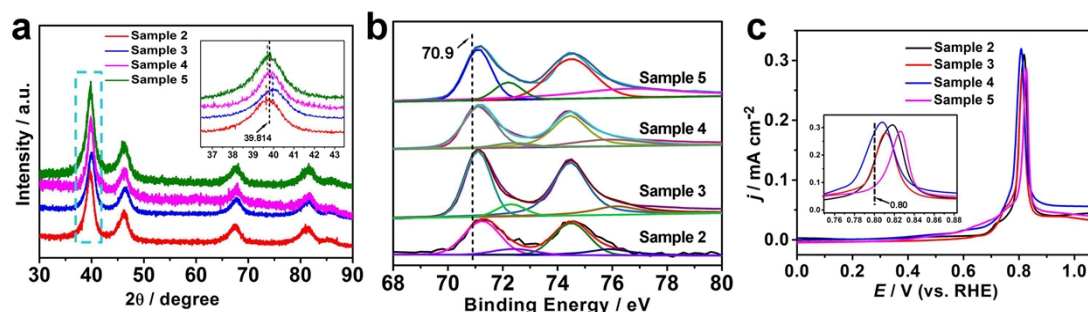

Figure S8. XRD patterns (a), XPS spectra (b) and CO stripping curves (c) of four control samples (sample 2, sample 3, sample 4 and sample 5). Insets in Fig. S8a and S8c are enlarged regions marked by cyan squares. The locations of black dash lines in Fig. S8a-c are the corresponding peak positions of dendritic Pt-Ni-P NPs (sample 1).

From Fig. S8a, we can see four characteristic diffraction peaks of fcc Pt. Notably, no other peaks appeared, indicating the crystal structure was not influenced by changing the ratio of the precursors. Inset of Fig. S8a shows that the peaks of four samples (sample 2, sample 3, sample 4 and sample 5) shift slightly relative to our PtNiP sample (sample 1) due to the different compositions in each sample. The XPS spectra (Fig. S8b) show that the Pt $4f2/7$ peaks of all the four samples are shifted to higher binding energies relative to our PtNiP sample. In other words, our PtNiP sample resulted in the biggest negative shift relative to PtNi sample (71.3 eV), which may be an optimized interaction of Pt, Ni and P. The CO stripping curves of four samples (Fig. S8c) indicate our PtNiP sample has the lowest peak potential, indicating that this material has the best antipoisoning property.
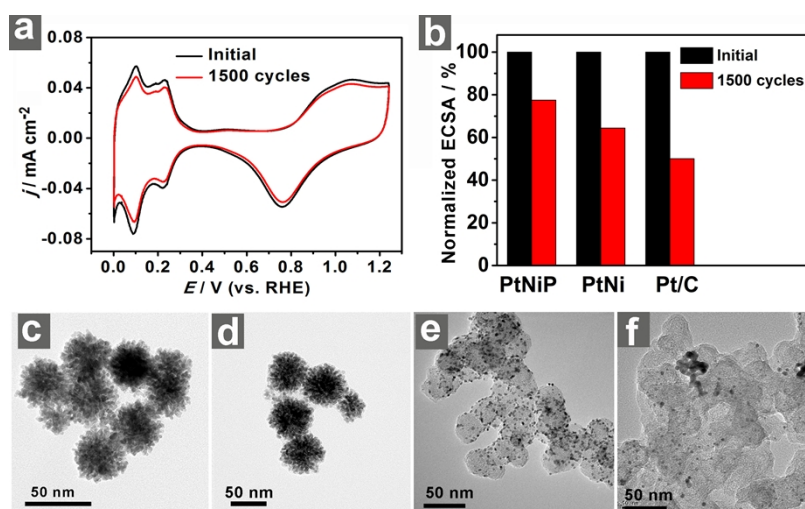

Figure S9. (a) CV curves for dendritic Pt-Ni-P alloy NPs after prolonged cycles of CV in an N_2-purged solution of 0.5 M H_2SO_4 at a scan rate of 50 mV s^{-1}. (b) Loss of ECSA of dendritic Pt-Ni-P alloy NPs, dendritic Pt-Ni alloy NPs and commercial Pt/C after potential sweep cycles. (c, d) Representative TEM images of dendritic Pt-Ni-P alloy NPs (c) and dendritic Pt-Ni alloy NPs (d) collected after 1500 cycles. (e, f) TEM images of commercial Pt/C catalyst before (e) and after (f) 1500 cycles.